Published in final edited form as:
Magn Reson Med. 2011 July ; 66(1): 248–254. doi:10.1002/mrm.22829.

Comparison of Lung T_2^* During Free-Breathing at 1.5T and 3.0T with Ultrashort Echo Time (UTE) Imaging

Jiangsheng Yu[1], **Yiqun Xue**[1], and **Hee Kwon Song**[1]

[1]Laboratory for Structural NMR Imaging, Department of Radiology University of Pennsylvania School of Medicine, Philadelphia, PA, United States

Abstract

Assessment of lung T_2^* may play an important role in the detection of structural and functional changes caused by lung diseases such as emphysema and chronic bronchitis. While T_2^* measurements have been conducted in both animals and humans at 1.5T, studies on human lung at 3.0T have not yet been reported. In this work, ultrashort echo time (UTE) imaging technique was applied for the measurement and comparison of T_2^* values in normal human lungs at 1.5T and 3.0T. A 2D UTE pulse sequence was implemented and evaluated in phantom experiments, in which an eraser served as a homogeneous short T_2^* sample. For the in vivo study, five normal human subjects were imaged at both field strengths and the results compared. The average T_2^* values measured during free-breathing were 2.11(±0.27)ms at 1.5T and 0.74(±0.1)ms at 3.0T, respectively, resulting in a 3.0T/1.5T ratio of 2.9. Furthermore, comparison of the relaxation values at end-expiration and end-inspiration, accomplished through self-gating, showed that during normal breathing, differences in T_2* between the two phases may be negligible.

Keywords

lung imaging; T_2*; ultrashort echo time (UTE) imaging

The dependence of T_2^* on the magnetic susceptibility difference between the airway and lung tissue suggests that the parameter has the potential to characterize the morphometric structure of micro-architecture of lung at the alveolar level. Structural and functional changes occurring in various pulmonary disorders that change the dimensions, density and composition of lung alveolar tissue may be reflected in the T_2^* values. However, magnetic resonance imaging of lung parenchyma is challenging due to the inherent limitations from low proton density, relatively short T_2^* relaxation time and respiratory motion(1,2). The multi-level airway structure, in which water concentration is only ~30%, makes the achievable signal intrinsically lower than other organs. The extremely short T_2^* of lung also demands a fast signal acquisition following excitation before signal decays into the noise level. Respiratory motion can also cause ghosting artifacts and degrades the lung image quality.

While T_2^* measurements of the lungs have been conducted in both animals and humans at 1.5T, studies on human lung at 3.0T have not yet been reported. The magnetic susceptibility effect is linearly proportional to the B_0 field strength, which suggests it may be more sensitive to subtle lung pathologic changes and may have the advantage in detecting early stages of lung diseases. However, lung T_2^* at 3.0T is expected to be considerably shorter

Corresponding author: Hee Kwon Song, Ph.D., Department of Radiology, University of Pennsylvania, 1 Silverstein/MRI, 3400 Spruce St., Philadelphia, PA 19104, HeeKwon.Song@uphs.upenn.edu, Tel: 215-662-6265, Fax: 215-662-7263.

than that at 1.5T. The ultrashort T_2^* at 3.0T precludes the use of Cartesian-based sequences, even when optimized to achieve very short TEs. Originally proposed by Pauly et.al. to image very short T_2^* species, ultrashort echo time (UTE) imaging is based on radial k-space sampling of the free induction decay(3,4). The uniqueness of UTE is the self-refocusing RF excitation, in which a half-sinc RF pulse in conjunction with a pair of gradients with opposite polarity is used for slice selective excitation, and the slice profile after combination is that of the tradition full-sinc excitation. With the elimination of slice selective rewinding gradient and with the application of FID acquisition, the effective echo time, which is defined as the delay between the end of excitation and collection of center of k-space signal, can readily be reduced to less than 100 us.

In this work, we present a comparison of lung T_2^* measurements in normal human subjects at 1.5T and 3.0T with a 2D UTE pulse sequence. The UTE sequence utilizing the golden-angle view increment strategy is first briefly described in the following section. A phantom experiment with an eraser serving as homogeneous short-T_2^* phantom is then performed to evaluate the UTE sequence. In the in-vivo lung imaging experiments, five normal human subjects were imaged in the axial orientation at the two magnetic field strengths. Based on the measurements performed at multiple echo times, the T_2^* values measured during free-breathing were calculated in six anterior and posterior regions, and the results compared. In addition, T_2* values were compared at end-expiration and end-inspiration by utilizing the self-gating strategy to detect the respiratory cycle.

Materials and Methods

2D UTE sequence

A 2D UTE sequence was implemented on Siemens Sonata 1.5T and Trio 3.0T MRI systems. The ultrashort echo time was achieved with a combination of radial sampling and self-refocusing RF excitation techniques. As demonstrated in Fig.1, the radial sampling techniques include an FID radial acquisition and ramp sampling. The self-refocusing RF excitation technique utilizes the half-sinc RF pulse excitation as well as the variable rate excitation (VERSE) methodology to play out the RF during the ramp down period(5,6).

The 2D UTE sequence is derived from a FLASH sequence with radial acquisition implemented by removing the Cartesian phase encoding gradient and rotating the readout direction in the imaging plane. To further reduce the achievable echo time, ramp sampling is utilized with the ramp-up time fixed at 150us. With a sampling dwell time of 3us (at 3.0T), 50 of the 256 samples were collected during the ramping period. Fig.1 also shows the data acquisition (ADC) was turned on 30us in advance of the readout gradient, and the k-space center was oversampled by 10 points at 3.0T. For excitation a two-side-lobe half-sinc RF pulse of 512us duration was used. With a fixed 150us ramp-down time of slice selective gradient, the RF pulse duration was stretched to 587us (=512us+75us) by VERSE technique. A half-Hamming filter was also applied to improve the smoothness of the slice profile.

With a combination of radial sampling and self-refocusing RF excitation techniques, the minimum echo time (TE) achievable is ultimately limited by the hardware dead time between the RF transmitter and the receiver of the scanner. We obtained 50us and 30us TEs at the Siemens 1.5T Sonata and 3.0T Trio MRI systems, respectively. View angle increment of 137.51°, which is the golden angle corresponding to half k-space projection acquisitions, advanced successive views during the measurements(7). The desirable feature of the golden angle view increment scheme used in the measurements is that the azimuthal sampling is approximately uniform for an arbitrary number of consecutive views at an arbitrary temporal position(7,8). Therefore the golden angle scheme allows reconstruction of images at

different respiratory phases, e.g. the end-expiration or end-inspiration, by choosing the corresponding angular view sets as determined by self-gating (7,8).

Phantom experiments

The 2D UTE sequence was evaluated with phantom experiments in which an eraser served as a homogeneous short-T_2^* phantom. The material of the specific eraser used consisted of polymers of styrene, ethylene, propylene and butylene subunits, and its dimensions were 100x100x20 mm^3. The choice of an eraser as the phantom is based on the assumption that the material's proton T_2^* relaxation times closely match those of the water protons in lung parenchyma. The following imaging parameters were used: field of view (FOV)= 300 mm; slice thickness=10 mm; TR=10 ms; flip angle=15°; receiver bandwidth=651 Hz/pixel for 1.5T (1302 Hz/pixel for 3.0T). As a part of this evaluation, we also examined the goodness of the slice excitation profile by rotating the imaging plane such that it was perpendicular to the slice selection plane.

In-vivo experiments

The lungs of five healthy male volunteers (aged 30~41) were imaged on both scanners using the transmit/receive body coil. The study was approved by the institutional review board and all subjects gave informed consent. The subjects were scanned in the supine position during free breathing. Single slice axial images were acquired with the 2D UTE sequence with the following parameters: FOV=300mm; Slice thickness=20mm; TR=10ms; Flip angle=7 degrees; Readout points=256. The readout bandwidth was 651Hz/pixel for 1.5T. To reduce the image blurring effect caused by faster signal decay, a higher bandwidth of 1302 Hz/pixel was used at 3.0T. A series of eight TE values were used in the experiments: [0.05, 0.2, 0.4, 0.6, 0.8, 1.0, 1.2, 1.4](ms) at 1.5T and [0.03, 0.1, 0.2, 0.3, 0.4, 0.5, 0.6, 0.7](ms) at 3.0T. Ten thousand angular views were acquired for a scan time of 3.4 minutes at each echo time.

Data processing

To reconstruct the images from radial k-space data, an accelerated regridding technique was implemented in MATLAB (Mathworks Inc., Natick, MA, USA). The regridding technique was proposed by Greengard et.al., in which an accelerated algorithm was developed for nonuniform Fast Fourier Transform (nuFFT)(9).

In the eraser phantom experiments, a single region-of-interest (ROI) was selected for the T_2^* measurements. During data processing for in-vivo experiments, the left and right lungs were first manually segmented. The images were then thresholded at 40% of the maximum intensity based on the first echo image to exclude large blood vessels to ensure T_2^* was measured for lung parenchyma. After segmentation, a voxel-by-voxel T_2^* fitting was performed by applying mono-exponential fitting to the signals of multiple TEs. In the fitting for 1.5T, the first point was excluded due to signal irregularities in some of the scans (the signal was lower than the second point), possibly caused by hardware jittering or insufficient receiver dead time. Prior to exponential fitting, the signals were first bias-corrected from the background noise(10,11)

$$S_n = \sqrt{\bar{S}_n^2 - \sigma^2}$$

where $\bar{S}_n$ and S_n denote the signal intensities before and after the correction, respectively, and σ represents the noise, which can be estimated as $\sigma = \sqrt{\frac{2}{\pi}}\bar{M}$, where $\bar{M}$ is the mean value of a 5x5 background region where no signal are present.

In addition, T_2* at end-expiration and end-inspiration were compared to determine whether significant differences between the two phases can be measured during normal breathing. To this end, radial self-gating was performed by observing the signal variations of data at k-space center to detect the respiratory cycle(7,8). Both magnitude and phase of the signal were first detected, followed by detection of the peaks and valleys, corresponding to end-expiration and end-inspiration, respectively. T_2* maps were subsequently constructed separately for both phases and the results compared.

Results

Phantom experiments

Figure 2 (a)-(c) shows the eraser phantom images acquired at TE= 0.05ms, 0.6ms and 3.0ms at 1.5T. Due to the ultrashort TEs (50us) obtained with the UTE sequence, the solid plastic casing of the coil is visible in the first two images (Fig.2(a) and (b)) and is characterized by a faster T_2^* decay rate than that of the eraser phantom. The ROI selected for T_2^* measurement is depicted as a dotted square box in Figure 2 (c). The imaged slice profile is shown in Figure 2 (d) and indicates that good slice-profile matching was achieved for the paired half-sinc excitations in the UTE sequence. Figure 3 (a) plots the measured points and the fitted T_2^* curves for the ROI at the two field strengths. The average T_2^* of the eraser phantom is 2.06ms at 1.5T and 1.55ms at 3.0T. Since the eraser phantom is essentially homogeneous, unlike the lung where tissue/air interface causes relaxation to be affected by the magnetic susceptibility differences, a linear relationship between the relaxation rate (R_2* = 1/T_2*) and field strength is not expected.

In-vivo experiments

To quantify the regional variations of T_2^* in the lungs, three regions from anterior to posterior were manually segmented for each side of the lungs in the T_2^* maps. Table 1 lists the T_2^* values in the six regions (anterior, middle and posterior regions of each lung) of the five subjects at 1.5T and 3.0T. The overall average T_2^* was 2.11(±0.27)ms and 0.74(±0.1)ms at 1.5T and 3.0T, respectively. The average T_2^* at 1.5T is close to the reported value of 1.8 ms reported in literature(12,13). The ratio of average T_2^* at the two field strengths is 2.9, which is larger than the ratio of the two field strengths. It is interesting to note that the middle regions (2 and 5) of the lungs have lower T_2^* value than the anterior and posterior regions at both field strengths. This observation is also in agreement with previous findings(12,14).

Figures 4 (a)-(c) show the lung images at TE= 0.03ms, 0.2ms and 0.6ms at 3.0T. Figure 4 (e) labels the six regions used for T_2^* calculations in Table 1. Figures 4 (f)-(g) show the corresponding lung images at 1.5T at the same latter two echo times to demonstrate a more slowly decaying signal as compared with 3.0T. Figures 4 (d) and (h) are the voxel-by-voxel fitted T_2^* maps for 3.0T and 1.5T. Since only normal subjects were included in this study, only small variations in T_2^* maps are observed. To illustrate the exponential fitting processing, Figure 3 (b) plots the measured points and the fitted curves of a randomly selected pixel in one of the regions at the two field strengths for one subject. The signal-to-noise ratio (SNR) in the vertical axis is defined as the mean value of the ROI signal intensity over the mean value of background noise.

The average SNR of the first image acquired with the shortest TE was 11.4 at 1.5T and 11.5 at 3.0T. Although the SNR at 3.0T is expected to be higher than that at 1.5T, some of the gain is reduced due to a higher acquisition bandwidth and longer T_1 at the higher field strength.

The radial acquisition strategy provides an advantage when imaging moving objects, as motion mainly leads to blurring rather than ghosting, and further, as self-gating can be utilized(8). As shown in Fig. 5 (a), when echo time is short (TE=0.03ms), the respiratory cycle can be observed by examining either the signal magnitude or phase at k-space center of consecutive views. However, at long echo times (for example, TE=0.7ms), the respiratory cycle can only be observed in the signal phase (Fig. 5 (c)). The inability to detect the respiratory cycle in the magnitude curve is possibly due to reduced magnitude signal from the lungs at long TEs. Following the detection of the peaks and valleys of the phase curves, lung images at both end-inspiration and end-expiration were separately reconstructed by utilizing temporal windows which span approximately one-third of each respiratory cycle. A voxel-by-voxel based fitting showed that the mean T_2^* values for end-inspiration and end-expiration are 0.80(±0.09)ms and 0.75(±0.04)ms at 3.0T, and 2.11(±0.16)ms and 2.22(±0.28)ms at 1.5T, respectively. Compared to overall T_2^* values 2.11(±0.27)ms at 1.5T and 0.74(±0.1)ms at 3.0T, no significant differences were observed between the two respiratory phases under normal breathing.

Discussion and Conclusion

Based on Case's model(15), the inflated lung can be simulated as a collection of air cavities (the alveoli) embedded in a water-like medium (the lung tissue). In an external magnetic field, each air-filled alveoli acts like a magnetic dipole due to the susceptibility difference between air and water. The field perturbation is then expected to be proportional to the external field strength. Although the variations in the dimensions, distribution and tissue density of alveoli in lung complicate the problem and make the determination of perturbated field at any local point difficult, the overall effects of magnetic susceptibility is expected to be linear to the B_0 field strength. This suggests that an approximate ratio of two in the average T_2^* values should be observed in MR imaging of lung at 1.5T and 3.0T. However, our measurement shows a ratio of 2.9. One possible reason for a larger reduction in T_2^* at 3T, exceeding the predicted factor of two, is the non-linear dependence of the signal decay rate on the background gradient as spins move through an inhomogeneous field. It has been shown that the signal decay rate due to diffusion in an inhomogeneous field is proportional to the square of the gradient(16). Although flow through the pulmonary vasculature is not identical to diffusion, movement of spins through quasi-random distribution of field perturbations in the lungs may create similar loss of phase coherence among the spins. Since these gradients are effectively doubled at the higher field strength, super-linear increase in relaxation rate may be expected.

Table 1 shows that the T_2^* ratios among different lung regions and subjects are not as consistent as one might expect. There are two possible explanations for the observed variations. First, there may be differences among different regions in the degree of flow-related effects as explained previously, which may artifactually augment the ratios by different amounts. Second, although we have tried our best in the segmentation of the lungs and exclusion of vessels, this process is likely to have been imperfect causing additional variations.

Although T_2^* is shorter at 3T, one potential benefit of the higher field is the enhanced sensitivity to changes in T_2^*. If the change in the transverse relaxation rate due to disease is susceptibility-dependent, this change is expected to scale with field, favoring higher field imaging. However, this advantage is realized only if the within-group variation in the measured T_2^* is dominated by measurement error rather than by inherent variability of T_2^* (e.g., due to variations in structure) within the group(17). More rapid signal decay may also limit the choice in pulse sequence one can use for making the measurement. For the lungs, for example, an optimized Cartesian gradient echo sequence has been used previously for

T_2^* assessment at 1.5T, but such measurement would be more difficult at 3T due to the enhanced signal decay.

While it is generally accepted that higher fields offer enhanced SNR, one must take into account that T_1 typically also increases with field, reducing the potential signal gain, particularly in short TR applications. In addition, when imaging the lungs or other tissues strongly characterized by susceptibility-related effects, it may be desirable to use higher receiver bandwidths to account for enhanced line broadening and image blurring. Use of higher bandwidths, however, will increase image noise (as the square root of receiver bandwidth). As shown in Fig. 3(b), these two factors in conjunction may have nearly completely offset the achievable gain in SNR at 3T.

In our in-vivo experiments, axial planes were chosen for lung T_2^* measurements as other have previously done (12,18). Lung imaging in other planes (sagittal or coronal) have also been reported in literature to investigate the spatial variations and heterogeneities of T_2* and density of the lungs(14,19,20). As we were careful to choose a consistent location using a slice thickness of 20mm (at the center of heart), any T_2^* variations due to lung tissue displacement is expected to be minor. Our measurements in effect reflect an average T_2^* value of the lung tissue that may have moved in/out of the prescribed slice location.

The long scan times we have used, on the order of 3 minutes per scan, is not strictly necessary. However, one of our goals was to demonstrate that T_2* measurements can be made while the subjects are free-breathing. This may be beneficial in patients who may have difficulty with breath-holding for any prolonged periods of time. In addition, as different echo times typically require separate breath-holding, misregistration among different echo times are possible with breath-held studies. Our method precludes the need for breath-held scans. Also, in light of recent interests in radial self-gating for motion compensation, our work demonstrates that self-gating can be used to generate lung T_2* maps at either end-expiratory or end-inspiratory stages of normal breathing. In addition, while shorter scan times are possible with our technique, the spatial resolution would have to be subsequently reduced due to reduced SNR. While high spatial resolution was not required for the study, the work demonstrates that enhanced resolution imaging of the lungs is indeed possible. This may be of benefit in future studies evaluating focal diseases or lesion heterogeneity.

Although a previous study by Theilmann, et al. demonstrated significant differences in lung T_2* at different breath-held positions(19), our finding that there is negligible difference between end-expiration and end-inspiration under normal breathing is not surprising. Theilmann's study compared T_2* values at three different lung volumes: Total lung capacity (T_2* = 1.2 ms), functional residual capacity (T_2* = 1.8 ms), and residual volume (T_2* = 2.0 ms). According to ref. 21, the volumes of air for these three respiratory positions in a healthy male are 6.0, 2.4, and 1.2 liters, respectively, while the tidal volume (amount of air breathed in or out during normal breathing) is about 0.5L(21). Thus, during normal breathing, the volume of air moving in and out of the lungs is relatively small compared to the volume at various breath-held positions studied previously. Roughly assuming a linear relationship between lung volume and T_2*, we estimate that a 0.5L difference in volume would lead to < 0.1 ms difference in T_2*, a figure too small to differentiate in our study with limited number of subjects and achievable SNR.

In summary, this work compares lung T_2^* at 1.5T and 3.0T. A 2D UTE sequence was implemented to achieve an ultrashort echo time well below 100us at 1.5T and 3.0T. In normal human subjects, the average T_2^* values of the lungs were 2.11(±0.27)ms at 1.5T and 0.74(±0.1)ms at 3.0T, respectively. The ratio of average T_2^* at the two field strengths is 2.9, greater than the theoretically predicted value of two. Furthermore, comparison of the

relaxation rates at end-expiration and end-inspiration showed that during normal breathing, differences in T_2* between the two phases may be negligible.

Acknowledgments

Grants: This work is supported by NIH R01-CA125226.

References

1. Gewalt SL, Glover GH, Hedlund LW, Cofer GP, MacFall JR, Johnson GA. MR microscopy of the rat lung using projection reconstruction. Magn Reson Med. 1993; 29(1):99–106. [PubMed: 8419748]
2. Bergin CJ, Pauly JM, Macovski A. Lung parenchyma: projection reconstruction MR imaging. Radiology. 1991; 179(3):777–781. [PubMed: 2027991]
3. Pauly, JCSND. Slice selective excitation for very short T2 species. Presented at the Ninth Annual Scientific Meeting and Exhibition of the Society of Magnetic Resonance in Medicine; August:18–27; New York: 1990.
4. Robson MD, Gatehouse PD, Bydder M, Bydder GM. Magnetic resonance: an introduction to ultrashort TE (UTE) imaging. Journal of computer assisted tomography. 2003; 27(6):825–846. [PubMed: 14600447]
5. Aranee Techawiboonwong HKSaFWW. In vivo MRI of submillisecond T2 species with two-dimensional and three-dimensional radial sequences and applications to the measurement of cortical bone water. NMR Biomed. 2008; 21:59–70. [PubMed: 17506113]
6. Conolly S, Nishimura D, Macovski A, Glover G. Variable-Rate Selective Excitation. Journal of Magnetic Resonance. 1988; 78(3):440–458.
7. Winkelmann S, Schaeffter T, Koehler T, Eggers H, Doessel O. An optimal radial profile order based on the Golden Ratio for time-resolved MRI. IEEE transactions on medical imaging. 2007; 26(1): 68–76. [PubMed: 17243585]
8. Lin W, Guo J, Rosen MA, Song HK. Respiratory motion-compensated radial dynamic contrast-enhanced (DCE)-MRI of chest and abdominal lesions. Magn Reson Med. 2008; 60(5):1135–1146. [PubMed: 18956465]
9. Greengard L, Lee JY. Accelerating the nonuniform fast Fourier transform. Siam Review. 2004; 46(3):443–454.
10. Gudbjartsson H, Patz S. The Rician distribution of noisy MRI data. Magn Reson Med. 1995; 34(6): 910–914. [PubMed: 8598820]
11. Henkelman RM. Measurement of signal intensities in the presence of noise in MR images. Medical physics. 1985; 12(2):232–233. [PubMed: 4000083]
12. Hatabu H, Alsop DC, Listerud J, Bonnet M, Gefter WB. T2* and proton density measurement of normal human lung parenchyma using submillisecond echo time gradient echo magnetic resonance imaging. European journal of radiology. 1999; 29(3):245–252. [PubMed: 10399610]
13. Pracht ED, Arnold JF, Wang T, Jakob PM. Oxygen-enhanced proton imaging of the human lung using T2. Magn Reson Med. 2005; 53(5):1193–1196. [PubMed: 15844155]
14. Hopkins SR, Henderson AC, Levin DL, Yamada K, Arai T, Buxton RB, Prisk GK. Vertical gradients in regional lung density and perfusion in the supine human lung: the Slinky effect. J Appl Physiol. 2007; 103(1):240–248. [PubMed: 17395757]
15. Case TA, Durney CH, Ailion DC, Cutillo AG, Morris AH. A Mathematical-Model of Diamagnetic Line Broadening in Lung-Tissue and Similar Heterogeneous Systems - Calculations and Measurements. Journal of Magnetic Resonance. 1987; 73(2):304–314.
16. Carr HY, Purcell EM. Effects of Diffusion on Free Precession in Nuclear Magnetic Resonance Experiments. Physical Review. 1954; 94(3):630–638.
17. Song HK, Wehrli FW, Ma J. Field strength and angle dependence of trabecular bone marrow transverse relaxation in the calcaneus. J Magn Reson Imaging. 1997; 7(2):382–388. [PubMed: 9090595]

18. Bergin CJ, Glover GH, Pauly JM. Lung parenchyma: magnetic susceptibility in MR imaging. Radiology. 1991; 180(3):845–848. [PubMed: 1871305]

19. Theilmann RJ, Arai TJ, Samiee A, Dubowitz DJ, Hopkins SR, Buxton RB, Prisk GK. Quantitative MRI measurement of lung density must account for the change in T(2) (*) with lung inflation. J Magn Reson Imaging. 2009; 30(3):527–534. [PubMed: 19630079]

20. Hatabu H, Gaa J, Tadamura E, Edinburgh KJ, Stock KW, Garpestad E, Edelman RR. MR imaging of pulmonary parenchyma with a half-Fourier single-shot turbo spin-echo (HASTE) sequence. European journal of radiology. 1999; 29(2):152–159. [PubMed: 10374663]

21. West, J. Respiratory physiology: the essentials. Baltimore, MD: Lippincott Williams & Wilkins; 1999.

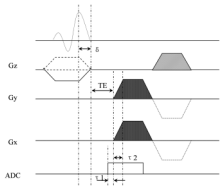

Figure 1.

Diagram of the 2D UTE sequence for lung T_2* measurement. The sequence combines FID radial acquisition, half-sinc RF pulse excitation, ramp sampling and VERSE techniques to achieve an ultrashort echo time below 100us. δ (150us): ramp-down time of slice selective gradient; τ1 (30us): duration of ADC in advance of the readout gradient; τ2 (150us): ramp-up time of the readout gradient.

Figure 2.
Eraser phantom experiment evaluating the 2D UTE sequence for short T_2* measurements. (a)-(c) are images acquired at 1.5T with UTE sequence at TE = 0.05, 0.6, 3.0ms, respectively. The region-of-interest (ROI) selected for T_2* measurement is depicted as a dotted square region in (c). (d) shows the slice profile.

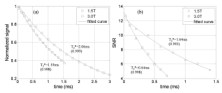

Figure 3.
Signal decay vs. echo time for the (a) eraser phantom and (b) a voxel in lung region 2 of subject 2 at 1.5T and 3.0T.

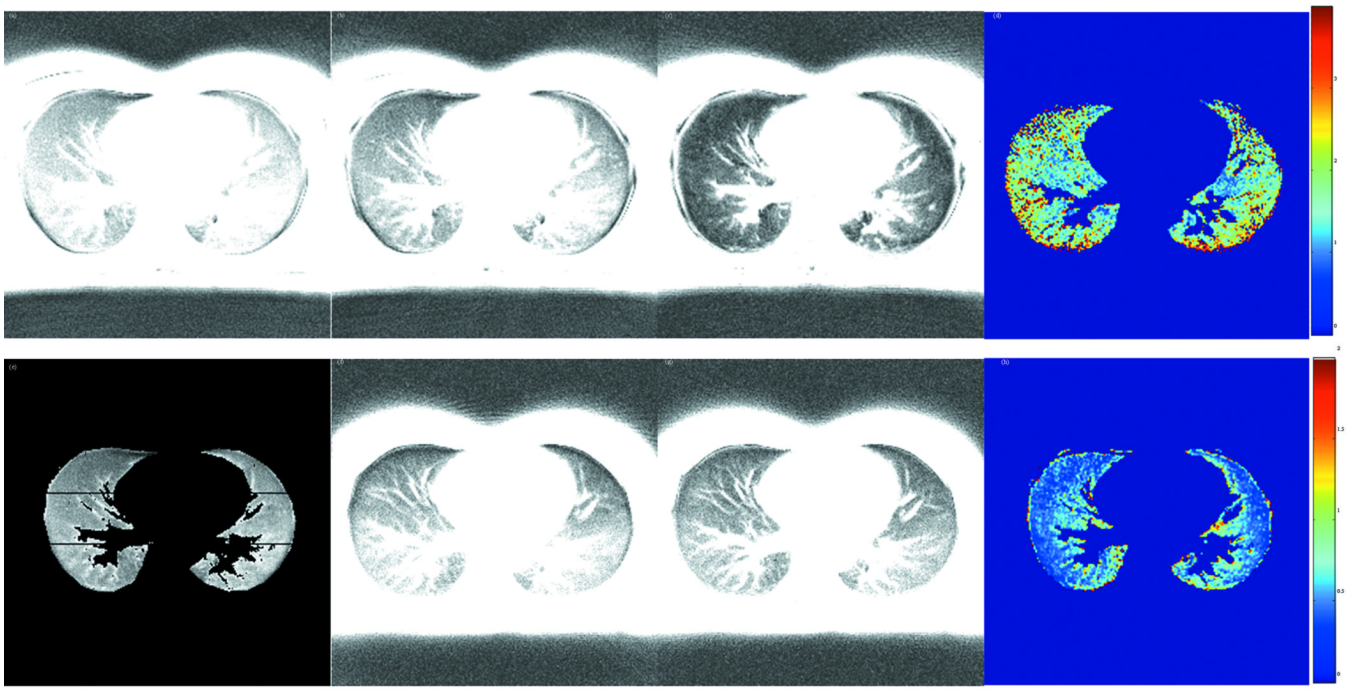

Figure 4.
Lung images of subject 2 acquired with UTE sequence at 3.0T and 1.5T. (a)-(c) are images of TE = 0.03, 0.2, and 0.6ms at 3.0T. (f)-(g) are images of TE = 0.2, and 0.6ms at 1.5T. (d) and (h) are the voxel-by-voxel fitted T_2^* maps for 3.0T and 1.5T, respectively. (e) shows the six regions of the lungs in Table 1 where the T_2^* values are listed.

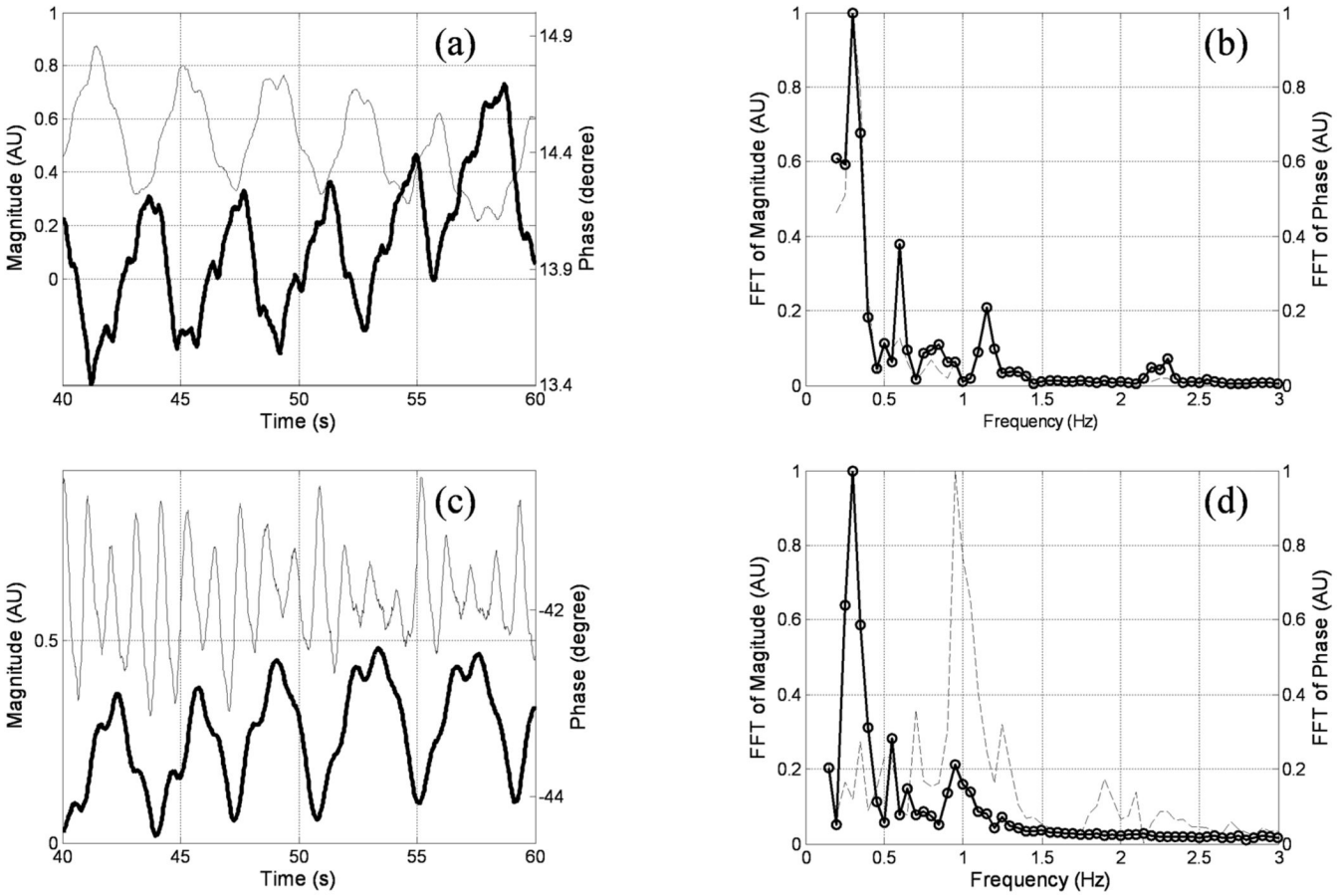

Figure 5.

Time evolution of signal magnitude and phase at the center of k-space acquired with the 2D UTE sequence during free breathing for subject 2 at 3.0T. (a) and (c) show the signal curves at TE = 0.03 and 0.7ms (phase in bold curves), respectively. (b) and (d) are the corresponding FFT curves in the frequency domain. At TE = 0.03, the respiratory cycle can be clearly observed in (b) as a peak around 0.25Hz in both magnitude (dotted curve) and phase (circled curve) spectra; while in (d) the respiratory cycle can only be observed in the phase spectrum. The peak near 1Hz in magnitude spectrum corresponds to the cardiac cycle.

Table 1

List of average T_2* values (unit ms) of the six lung regions for the five normal subjects at 3.0T and 1.5T. The corresponding regions are labeled in Fig. 4(e). The last column is the global average T_2* over the entire lung for each subject at the two field strengths. The T_2* values listed here were measured over the entire respiratory cycle during free breathing.

		Region L1	Region L2	Region L3	Region R1	Region R2	Region R3	Average
Subject 1	**1.5T**	2.29	1.76	2.50	2.40	2.04	2.94	2.38
	3.0T	0.66	0.74	0.87	0.81	0.41	1.25	0.83
	Ratio	*3.47*	*2.38*	*2.87*	*2.96*	*4.98*	*2.35*	*2.87*
Subject 2	**1.5T**	2.22	1.71	1.99	3.18	1.68	2.18	2.26
	3.0T	0.58	0.84	0.60	0.78	0.73	0.59	0.60
	Ratio	*3.83*	*2.04*	*3.32*	*4.08*	*2.30*	*3.69*	*3.77*
Subject 3	**1.5T**	2.13	2.02	2.12	1.64	1.59	2.19	1.93
	3.0T	0.71	0.43	0.88	0.69	0.57	0.79	0.74
	Ratio	*3.00*	*4.70*	*2.41*	*2.38*	*2.79*	*2.77*	*2.61*
Subject 4	**1.5T**	1.57	1.39	2.08	1.66	1.56	1.66	1.74
	3.0T	0.55	0.66	0.92	1.03	0.81	0.91	0.83
	Ratio	*2.85*	*2.11*	*2.26*	*1.61*	*1.93*	*1.82*	*2.10*
Subject 5	**1.5T**	2.14	2.11	2.39	2.43	1.77	2.19	2.24
	3.0T	0.72	0.63	0.79	0.99	0.74	0.78	0.68
	Ratio	*2.97*	*3.35*	*3.03*	*2.45*	*2.39*	*2.80*	*3.29*